Hindawi
Journal of Nanomaterials
Volume 2022, Article ID 5286921, 20 pages
https://doi.org/10.1155/2022/5286921

Research Article

Darcy-Forchheimer 3D Flow of Glycerin-Based Carbon Nanotubes on a Riga Plate with Nonlinear Thermal Radiation and Cattaneo-Christov Heat Flux

S. Eswaramoorthi,[1] **K. Loganathan**,[2,3] **Reema Jain**,[2] **and Sonam Gyeltshen**[4]

[1]*Department of Mathematics, Dr. N.G.P. Arts and Science College, Coimbatore, Tamil Nadu, India*
[2]*Department of Mathematics and Statistics, Manipal University Jaipur, Jaipur, Rajasthan, India*
[3]*Research and Development Wing, Live4Research, Tiruppur-638106, Tamilnadu, India*
[4]*Department of Humanities and Management, Jigme Namgyel Engineering College, Royal University of Bhutan, Dewathang, Bhutan*

Correspondence should be addressed to S. Eswaramoorthi; eswaran.bharathiar@gmail.com and Sonam Gyeltshen; sonamgyeltshen@jnec.edu.bt

Received 7 January 2022; Revised 13 February 2022; Accepted 6 April 2022; Published 5 May 2022

Academic Editor: Taza Gul

The current investigation deliberates the consequence of the glycerin-based carbon nanotubes with velocity slip in Darcy-Forchheimer porous medium on a convectively heated Riga plate. The Fourier heat flux theory was replaced by the Cattaneo-Christov theory. Moreover, nonlinear facets of radiation are also included in the energy expression, and this creates the energy expression which becomes highly nonlinear. The governing flow problems are altered into an ODE model with the help of suitable variables. The reduced models are solved numerically by applying MATLAB bvp4c theory and analytically by HAM idea. The impact of diverse physical parameters on velocity, temperature, skin friction coefficients, local Nusselt number, entropy generation, and Bejan number are scrutinized through tables and graphs. It is seen that both directions of fluid motion elevate when raising the modified Hartmann number, and it diminishes when escalating the quantity of the Forchheimer number and porosity parameter. The fluid warmth grows when the higher magnitude of the Biot number and heat generation/consumption parameter, and it downturns when enriching the thermal relaxation time parameter. The entropy generation slumps when heightening the slip parameter, whereas it improves when rising the radiation parameter. The Bejan number upturns when upgrading the Biot number and heat generation/consumption parameter.

1. Introduction

The fluid thermal conductivity performs a significant role in many industrial and engineering procedures, especially in the cooling and heating of thermal systems. Conventional fluids like oil, ethylene glycol, and water transfer less heat due to weaker thermal conductivity. Nowadays, several scientists put more effort into upgrading the fluid thermal conductivity. The submersion of nanometer particles like oxide, carbides, metal oxides, carbon nanotubes (CNTs), and graphite in conventional fluids is one of the easiest procedures for enhancing the fluid thermal conductivity. In particular, CNTs have superior power of enhancing thermal conductivity compared to other nanometer particles (see [1, 2]). The CNTs can be classified into SWCNTs and MWCNTs. Haq et al. [3] report the heat transfer analysis of an MHD viscous nanofluid flow on a stretching surface via carbon nanotubes. They noticed that the surface shear stress was high in engine oil-based CNTs than the ethylene glycol- and water-based CNTs. The outcome of nanofluid flow-

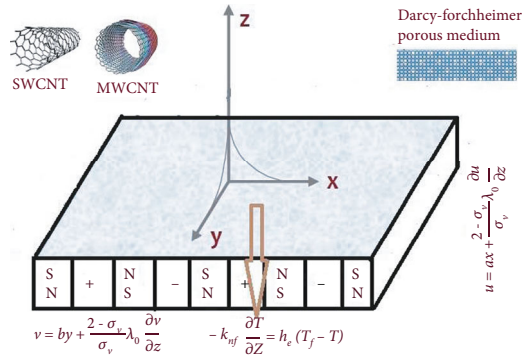

Figure 1: Physical configuration of the flow model.

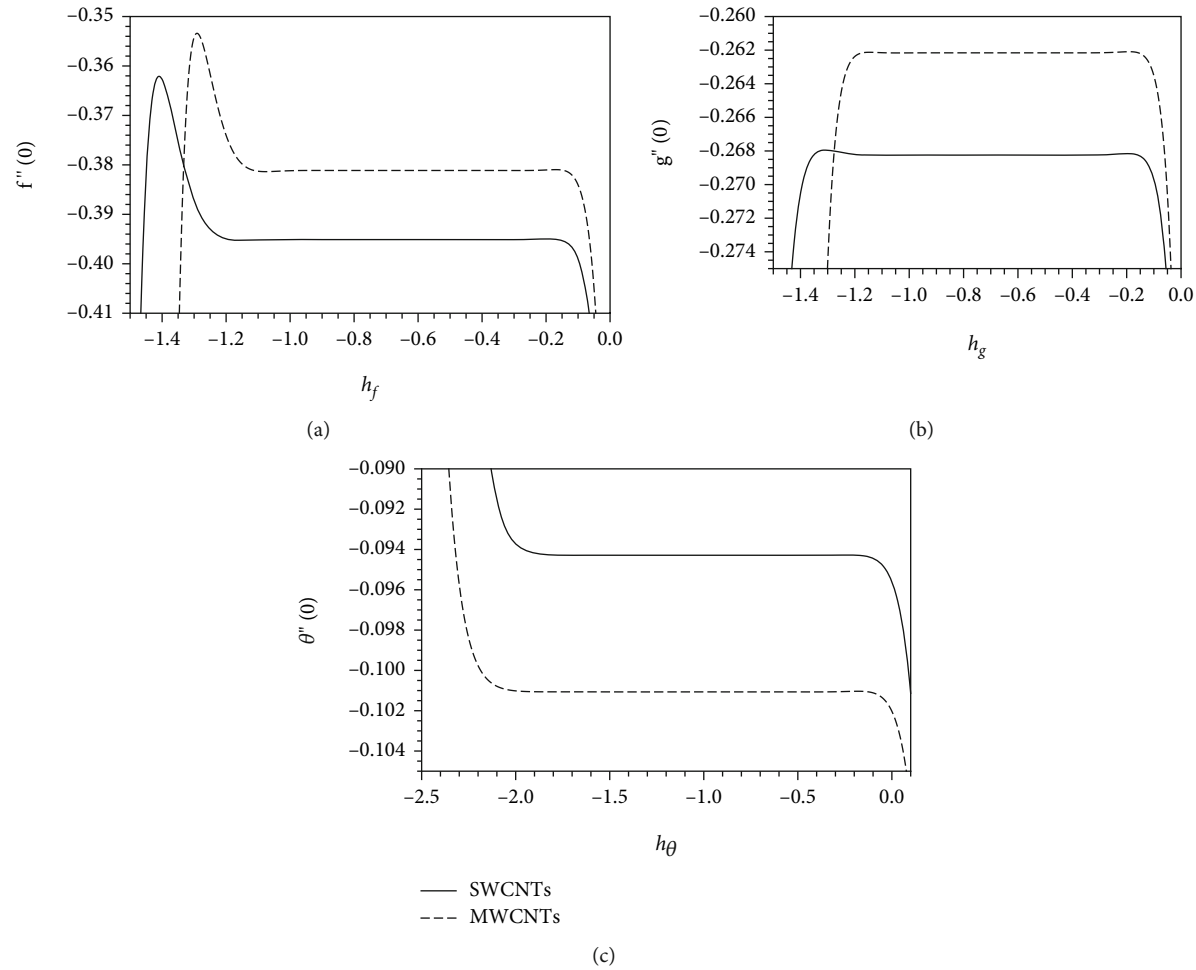

Figure 2: h-curves of (a) x-direction velocity, (b) y-direction velocity, and (c) nanomaterial volume fraction profiles for both nanotubes.

suspended CNTs with the presence of activation energy and binary chemical reaction on a non-Darcy porous medium was addressed by Lu et al. [4]. They exposed that the solid volume fraction of nanofluid enriches the fluid velocity. Rehman et al. [5] inspect the influence of SWCNTs on engine oil- and water-based 3D rotating fluid on a stretching sheet. They detected that engine oil-based fluid has a larger heat transfer gradient compared to water-based fluid.

Table 1: Physical properties.

Physical characteristics	SWCNTs	MWCNTs	Glycerin
k	6600	3000	0.286
ρ	2600	1600	1259.9
c_p	425	796	2427
Pr	–	–	6.78

Table 2: Order of approximations.

Order	SWCNTs			MWCNTs		
	$-f''(0)$	$-g''(0)$	$-\theta'(0)$	$-f''(0)$	$-g''(0)$	$-\theta'(0)$
1	0.391118	0.268199	0.093867	0.365128	0.259087	0.100429
5	0.395396	0.268234	0.094323	0.381107	0.262157	0.101120
10	0.395112	0.268247	0.094284	0.381126	0.262160	0.101061
14	0.395110	0.268247	0.094286	0.381132	0.262161	0.101066
15	0.395110	0.268247	0.094286	0.381132	0.262161	0.101066
20	0.395110	0.268247	0.094286	0.381132	0.262161	0.101066
25	0.395110	0.268247	0.094286	0.381132	0.262161	0.101066
30	0.395110	0.268247	0.094286	0.381132	0.262161	0.101066
35	0.395110	0.268247	0.094286	0.381132	0.262161	0.101066
40	0.395110	0.268247	0.094286	0.381132	0.262161	0.101066

Table 3: Comparison of $-Cfx\sqrt{\mathrm{Re}}$ and $-Cfy\sqrt{\mathrm{Re}}$ with Hayat et al. [56] with $\phi = \mathrm{Fr} = \lambda = \mathrm{Ha} = 0$.

c	$-Cfx\sqrt{\mathrm{Re}}$		$-Cfy\sqrt{\mathrm{Re}}$	
	Present	Ref. [56]	Present	Ref. [56]
0.0	1.00000	1.000000	0.00000	0.000000
0.3	1.05795	1.057955	0.243360	0.243360
0.5	1.09310	1.093094	0.465205	0.465205
0.8	1.14249	1.142488	0.866683	0.866680
1.0	1.17372	1.173722	1.173720	1.173723

MHD flow of SWCNTs and MWCNTs on a vertical cone with the convective heating condition was demonstrated by Sreedevi et al. [6]. They proved that the mass transfer gradient is lower in MWCNTs than in the SWCNTs for the varying values of nanoparticle volume fraction. Lu et al. [7] investigated the time-dependent squeezing flow of nanofluid suspended in CNTs with the Cattaneo-Christov theory. They have seen that the nanoparticle volume friction leads to slowing down the fluid temperature. The ferric oxide- and carbon nanotube water-based hybrid nanofluid on a wavy fluctuating rotating disk was discussed by Bilal et al. [8]. Their finding shows that both CNTs are enriching the fluid velocity. Gul et al. [9] discussed the impact of engine oil-based CNTs on a rotating disk with a magnetic field. They identified that the skin friction coefficient is high for MWCNTs than for the SWCNTs when changing the magnetic field parameter.

The fluid flow analysis through the porous medium is a salient feature in many industries, like porous bearings, crude oil production, fermentation processes, grain storage, and casting solidification. Many articles associated with porous space deal with implementing Darcy's law. The major demerit of this law is to apply only weaker porosity and lesser velocity problems. Most of the physical issues have uneven porosity and larger flow transportation. In this situation, Darcy's law is inadequate. Forchheimer [10] rectifies this difficulty by adding a square velocity term in the momentum expression. The forced convective flow of viscous fluid on a Darcy-Forchheimer porous shrinking sheet with multiple slip conditions was demonstrated by Bakar et al. [11]. They proved that the fluid temperature declines in the first solution and increases in the second solution for changing the porosity parameter. Umavathi et al. [12] explored the Darcy-Forchheimer-Brinkman flow of a nanofluid in a rectangular duct. They discovered that the fluid temperature exalts for more quantity of the Brinkman number. The repercussion of heterogeneous/homogeneous reactions of a Darcy-Forchheimer flow of water-based carbon nanotubes on a rotating disk was studied by Hayat et al. [13]. Their decisions show that the Forchheimer number reinforces the skin friction coefficient. Ramzan and Shaheen [14] investigated the effects of the nanofluid flow through carbon nanotubes on a Darcy-Forchheimer stretching surface. They disclosed that the inertia coefficient leads to aggrandising the fluid velocity. The Darcy-Forchheimer flow of MHD nanofluid on a nonlinear stretching surface was evaluated by Rasool et al. [15]. They found that the surface shear stress jumps for a higher Forchheimer number. Nayak et al. [16] implemented the Darcy-Forchheimer law for investing the flow analysis of copper-water nanofluid on a disk. The 2D flow of MHD couple stress hybrid nanofluid on a Darcy-Forchheimer porous medium was inspected by Saeed et al. [17]. They proved that the inertia coefficient (Fr) decimates the fluid velocity. Darcy-Forchheimer flow of ethylene glycol-based nanofluid on a curved stretching surface with Arrhenius activation energy was presented by Maraj et al. [18].

Heat transfer through radiation plays a pivotal role in many manufacturing processes, like glass blowing, rubber sheet production, nuclear power plants, and tinning of copper wires. Keeping these usages in mind, several researchers scrutinized radiative heat transfer in different physical situations. Mehmood et al. [19] encountered the consequences of the radiative flow of viscoplastic fluid on a porous sheet. They detected that the thermal boundary layer thickened when raising the radiation parameter. Thermally radiative MHD flow nanofluid on a stretching sheet with second-order slip condition was inspected by Mabood and Das [20]. They observed that the fluid temperature upturns for increasing the radiation parameter. Ramzan et al. [21] deliberated the influence of nonlinear thermal radiation and chemical reaction of an MHD nanofluid on a heated plate.

Table 4: The HAM and numerical values of $Cfx\sqrt{\mathrm{Re}}$ and $Cfy\sqrt{\mathrm{Re}}$ of SWCNTs for diverge values of λ, Fr, Ha, c, K, and ϕ.

λ	Fr	Ha	c	K	ϕ	SWCNTs			
						$Cfx\sqrt{\mathrm{Re}}$		$Cfy\sqrt{\mathrm{Re}}$	
						Numerical	Analytical	Numerical	Analytical
0	0.4	0.5	0.6	1	0.2	-0.628909	-0.628903	-0.927277	-0.92727
0.3						-0.717409	-0.717410	-1.042841	-1.042840
0.5						-0.765947	-0.765948	-1.102898	-1.102900
0.8						-0.827006	-0.827006	-1.176055	-1.176060
1						-0.861597	-0.861597	-1.216598	-1.216600
0.2	0	0.5	0.6	1	0.2	-0.654495	-0.654495	-0.987723	-0.987722
	0.5					-0.698291	-0.698291	-1.013220	-1.013222
	1					-0.734473	-0.734473	-1.036740	-1.036742
	1.5					-0.765175	-0.765175	-1.058400	-1.058405
	2					-0.791757	-0.791757	-1.078390	-1.078390
0.2	0.4	0	0.6	1	0.2	-0.811524	-0.811526	-0.995010	-0.995011
		0.3				-0.737372	-0.737372	-1.003201	-1.003200
		0.5				-0.690229	-0.690229	-1.008283	-1.008280
		0.8				-0.622351	-0.622351	-1.015440	-1.015440
		1				-0.578733	-0.578729	-1.019946	-1.019940
0.2	0.4	0.5	0.1	1	0.2	-0.673012	-0.673013	-2.161610	-2.161610
			0.3			-0.680479	-0.680478	-1.332389	-1.332390
			0.5			-0.687131	-0.687130	-1.082817	-1.082820
			0.8			-0.696063	-0.696063	-0.903290	-0.903291
			1			-0.701499	-0.701499	-0.830992	-0.830992
0.2	0.4	0.5	0.6	0	0.2	-1.689558	-1.689560	-2.237526	-2.237530
				1		-0.690229	-0.690229	-1.008283	-1.008280
				2		-0.444308	-0.444309	-0.672968	-0.672969
				3		-0.329252	-0.329232	-0.509501	-0.509500
0.2	0.4	0.5	0.6	1	0	-0.390100	-0.390100	-0.618400	-0.618399
					0.05	-0.446787	-0.446787	-0.692571	-0.692570
					0.1	-0.513787	-0.513787	-0.779871	-0.779870
					0.15	-0.593754	-0.593754	-0.883625	-0.883624
					0.2	-0.690229	-0.690229	-1.008283	-1.008280

They noticed that the heat transfer gradient escalates for enhancing the radiation parameter. The nonlinear thermal radiation effect on Cu-Al_2O_3-water-based hybrid nanofluid on the stretching surface was portrayed by Usman et al. [22]. They noticed that the local Nusselt number suppresses when there is more presence of nonlinear thermal radiation parameters. Waqas et al. [23] scrutinized the impact of nonlinear thermal radiation of a micropolar nanofluid with gyrotactic microorganisms. They uncovered that the fluid temperature grows for a high quantity of temperature ratio parameter. The series solution of time-dependent viscoelastic micropolar nanofluid with thermal radiation and Cattaneo-Christov heat/mass flux theory was derived by Khan et al. [24]. Li et al. [25] revealed the radiative flow of modified second-grade nanofluid with second-order slip conditions. They have seen that the temperature ratio parameter leads to the downfall of the heat transfer gradient. Few progress about thermal radiative flow can be found in Refs. ([26–29]).

In the past few decades, many authors have examined entropy generation in fluid flow and heat transfer on a surface. Various factors, like viscous dissipation, chemical reactions, friction forces, and diffusion, are responsible for creating entropy. The entropy generation of the thermal system damages the effective work and suppresses the system efficiency. In this situation, Bejan [30] created a new model named as Entropy Generation Minimization (EGM), which is useful to reduce the energy losses in heat transfer processes and enrich the system efficiency. The entropy analysis of a forced convective flow of MHD Casson fluid in a microchannel with radiation was presented by Makinde and Eegunjobi [31]. They noticed that the Bejan number elevates for high magnitudes of magnetic field parameter. Bhatti et al. [32] derived the numerical

Table 5: The HAM and numerical values of $Cfx\sqrt{\mathrm{Re}}$ and $Cfy\sqrt{\mathrm{Re}}$ of MWCNTs for diverge values of λ, Fr, Ha, c, K, and ϕ.

λ	Fr	Ha	c	K	ϕ	MWCNTs			
						$Cfx\sqrt{\mathrm{Re}}$		$Cfy\sqrt{\mathrm{Re}}$	
						Numerical	Analytical	Numerical	Analytical
0	0.4	0.5	0.6	1	0.2	-0.597692	-0.597688	-0.896045	-0.896037
0.3						-0.695638	-0.695639	-1.022917	-1.022920
0.5						-0.748363	-0.748363	-1.087344	-1.087340
0.8						-0.813778	-0.813779	-1.164709	-1.164710
1						-0.850433	-0.850433	-1.207141	-1.207150
0.2	0	0.5	0.6	1	0.2	-0.630797	-0.630796	-0.965518	-0.965518
	0.5					-0.673734	-0.673733	-0.990190	-0.990190
	1					-0.709390	-0.709390	-1.012999	-1.013000
	1.5					-0.739767	-0.739763	-1.034062	-1.034060
	2					-0.766154	-0.766163	-1.053545	-1.053550
0.2	0.4	0	0.6	1	0.2	-0.792587	-0.792588	-0.972431	-0.972433
		0.3				-0.715130	-0.715130	-0.980431	-0.980431
		0.5				-0.665811	-0.665810	-0.985407	-0.985407
		0.8				-0.594720	-0.594709	-0.992431	-0.992430
		1				-0.548995	-0.548938	-0.996860	-0.996859
0.2	0.4	0.5	0.1	1	0.2	-0.649036	-0.649035	-2.121875	-2.121870
			0.3			-0.656279	-0.656279	-1.304265	-1.304270
			0.5			-0.662776	-0.662775	-1.058626	-1.058630
			0.8			-0.671540	-0.671539	-0.882437	-0.882437
			1			-0.676890	-0.676889	-0.811676	-0.811676
0.2	0.4	0.5	0.6	0	0.2	-1.574918	-1.574920	-2.117896	-2.117900
				1		-0.665811	-0.665810	-0.985407	-0.985407
				2		-0.432015	-0.432023	-0.663082	-0.663083
				3		-0.321333	-0.321347	-0.503983	-0.503985
0.2	0.4	0.5	0.6	1	0	-0.390100	-0.390100	-0.618400	-0.618399
					0.05	-0.441792	-0.441791	-0.688175	-0.688175
					0.1	-0.503167	-0.503167	-0.770314	-0.770314
					0.15	-0.576723	-0.576723	-0.867974	-0.867974
					0.2	-0.665811	-0.665810	-0.985407	-0.985407

solution of radiative MHD Williamson nanofluid in a porous shrinking sheet with entropy generation. Rashidi et al. [33] deliberated the entropy analysis of MHD third-grade fluid on a stretching sheet. They found that the entropy generation exalts when escalating the Brinkman number. The 3D double-diffusive flow of power law fluid with entropy analysis was investigated by Zhu et al. [34]. Jain and Gupta [35] explored the 3D flow of water-based CNT nanofluid past a heated inclined porous stretching sheet with entropy generation. They exposed that the entropy generation number improves when growing the Biot and Reynolds numbers. The latest investigations for this concept are collected in Refs. [36–41].

The aforementioned literature studies divulge that none of them inspected the Darcy-Forchheimer flow of glycerin-based carbon nanotubes on a Riga plate subjected to heat absorption, slip, and convective heating condition. In addition, our study includes entropy generation through different flow parameters inside the boundary layer flow. Our findings may find the applications in thermal extrusion phenomenon, cooling processes, oceanography, missile technology, and movement of biological fluids. Also, entropy generation plays a vital role in controlling the heat transfer rate in the proximity of a surface.

2. Mathematical Formulation

Let us contemplate the 3D Darcy-Forchheimer flow of glycerin-based carbon nanotubes over a Riga plate. There are two kinds of CNTs, like SWCNTs (single-wall carbon nanotubes) and MWCNTs (multiwall carbon nanotubes), which are considered. Let us choose x- and y-axes along with the plate, and z is perpendicular to the plate. Let $u = ax$ and $v = by$ be the velocity components in x and y directions. The

Table 6: The HAM and numerical values of local Nusselt number for diverge values of Ha, c, K, ϕ, Hg, R, Bi, Γ, and Λ for both CNTs.

Ha	c	K	ϕ	Hg	R	Bi	Γ	Λ	$\frac{Nu}{\sqrt{\mathrm{Re}}}$ SWCNTs		MWCNTs	
									Numerical	Analytical	Numerical	Analytical
0	0.6	1	0.2	-0.4	0.6	0.6	0.1	1.2	0.613593	0.613593	0.617908	0.617909
0.3									0.614827	0.614827	0.619235	0.619236
0.5									0.615577	0.615577	0.620041	0.620040
0.8									0.616613	0.616610	0.621154	0.621144
1									0.617254	0.617245	0.621841	0.621819
0.5	0.1	1	0.2	-0.4	0.6	0.6	0.1	1.2	0.611117	0.611118	0.615224	0.615225
	0.3								0.613118	0.613119	0.617379	0.617381
	0.5								0.614813	0.614814	0.619213	0.619214
	0.8								0.616973	0.616971	0.621556	0.621550
	1								0.618229	0.618225	0.622918	0.622906
0.5	0.6	0	0.2	-0.4	0.6	0.6	0.1	1.2	0.623712	0.623714	0.628428	0.628455
		1							0.615577	0.615577	0.620041	0.620040
		2							0.612416	0.612419	0.616674	0.616679
		3							0.610610	0.610612	0.614730	0.614735
0.5	0.6	1	0	-0.4	0.6	0.6	0.1	1.2	0.858530	0.858694	0.858530	0.858694
			0.05						0.713177	0.713261	0.720184	0.720290
			0.1						0.659079	0.659103	0.665538	0.665574
			0.15						0.631681	0.631685	0.637077	0.637084
0.5	0.6	1	0.2	-0.4	0.6	0.6	0.1	1.2	0.615577	0.615577	0.620040	0.620041
				-0.2					0.604723	0.604726	0.609498	0.609511
				-0.1					0.596760	0.596745	0.601962	0.601933
				0					0.585550	0.585552	0.591691	0.591621
				0.1					0.567896	0.567951	0.576447	0.576599
				0.2					0.532889	0.532766	0.550123	0.550314
0.5	0.6	1	0.2	-0.4	0	0.6	0.1	1.2	0.539505	0.539505	0.538442	0.538442
					0.3				0.577581	0.577581	0.579289	0.579288
					0.5				0.602920	0.602920	0.606467	0.606467
					0.8				0.640862	0.640863	0.647156	0.647155
					1				0.671718	0.666112	0.674229	0.674228
0.5	0.6	1	0.2	-0.4	0.6	-0.6	0.1	1.2	-0.769998	-0.769998	-0.778918	-0.778920
						-0.3			-0.362449	-0.362449	-0.366205	-0.366205
						0			0	0	0	0
						0.3			0.324160	0.324160	0.326820	0.326819
						0.6			0.615577	0.615577	0.620041	0.620040
0.5	0.6	1	0.2	-0.4	0.6	0.6	0	1.2	0.610956	0.610956	0.614983	0.614983
							0.2		0.617979	0.617979	0.622673	0.622672
							0.4		0.622974	0.622975	0.628155	0.628154
							0.6		0.630976	0.630976	0.636956	0.636956
							0.8		0.636674	0.636675	0.643239	0.643239
0.5	0.6	1	0.2	-0.4	0.6	0.6	0.1	1	0.615308	0.615309	0.619724	0.619721
								1.3	0.615858	0.615860	0.620374	0.620379
								1.5	0.616463	0.616472	0.621096	0.621122
								1.8	0.617147	0.617132	0.621896	0.621931
								2	0.617859	0.617839	0.622685	0.622704

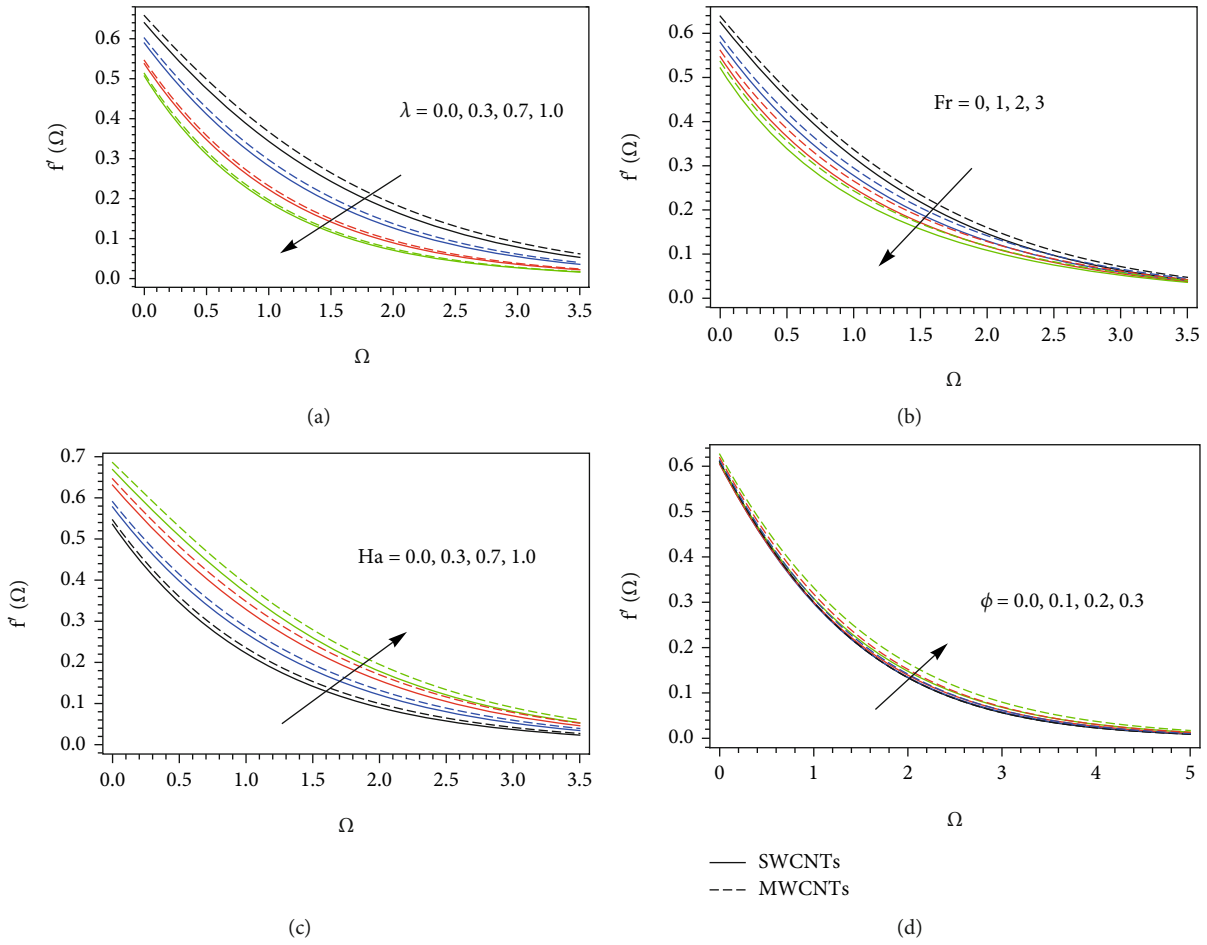

Figure 3: The x-direction velocity for distinct quantity of λ (a), Fr (b), Ha (c), and ϕ (d).

fluid behaves heat consumption or generation (see Rana et al. [42]). The nonlinear thermal radiation is taken into account. The Fourier heat flux model was replaced by the Cattaneo-Christov model (see Punith Gowda et al. [43]). The underneath of the plate was convectively heated fluid by hot fluid with temperature T_f, and this generates heat transfer coefficient h_c (see Figure 1). Under the above considerations, the governing flow expression is as follows (see Hayat et al. [44–45] and Zeeshan et al. [46]):

$$\frac{\partial u}{\partial x} + \frac{\partial v}{\partial y} + \frac{\partial w}{\partial z} = 0, \tag{1}$$

$$u\frac{\partial u}{\partial x} + v\frac{\partial u}{\partial y} + w\frac{\partial u}{\partial z} = \nu_{nf}\frac{\partial^2 u}{\partial z^2} - \frac{\nu_{nf}}{k_1^*}u - Fu^2 + \frac{\pi J_0 M}{8\rho_{nf}}\mathrm{Exp}\left[-\frac{\pi}{a_1}z\right], \tag{2}$$

$$u\frac{\partial v}{\partial x} + v\frac{\partial v}{\partial y} + w\frac{\partial v}{\partial z} = \nu_{nf}\frac{\partial^2 u}{\partial z^2} - \frac{\nu_{nf}}{k_1^*}v - Fv^2, \tag{3}$$

$$\begin{aligned} &u\frac{\partial T}{\partial x} + v\frac{\partial T}{\partial y} + w\frac{\partial T}{\partial z} \\ &= \alpha_{nf}\frac{\partial^2 T}{\partial z^2} + \frac{16\sigma^*}{3k^*\left(\rho c_p\right)_{n_f}}\left[T^3\frac{\partial^2 T}{\partial y^2} + 3T^2\left(\frac{\partial T}{\partial z}\right)^2\right] \\ &\quad + \frac{Q}{\left(\rho c_p\right)_{n_f}}\left(T - T_\infty\right) - \lambda\left[u^2\frac{\partial^2 T}{\partial x^2} + v^2\frac{\partial^2 T}{\partial y^2} + w^2\frac{\partial^2 T}{\partial z^2}\right. \\ &\quad + 2uv^2\frac{\partial^2 T}{\partial x\partial y} + 2vw\frac{\partial^2 T}{\partial x\partial y} + 2wu\frac{\partial^2 T}{\partial z\partial x} \\ &\quad + \left(u\frac{\partial u}{\partial x} + v\frac{\partial u}{\partial y} + w\frac{\partial u}{\partial z}\right)\frac{\partial T}{\partial x} \\ &\quad + \left(u\frac{\partial v}{\partial x} + v\frac{\partial v}{\partial y} + w\frac{\partial v}{\partial z}\right)\frac{\partial T}{\partial y} \\ &\quad \left. + \left(u\frac{\partial w}{\partial x} + v\frac{\partial w}{\partial y} + w\frac{\partial w}{\partial z}\right)\frac{\partial T}{\partial x}\right], \end{aligned} \tag{4}$$

with interacted boundary conditions (see Hayat et al. [45]

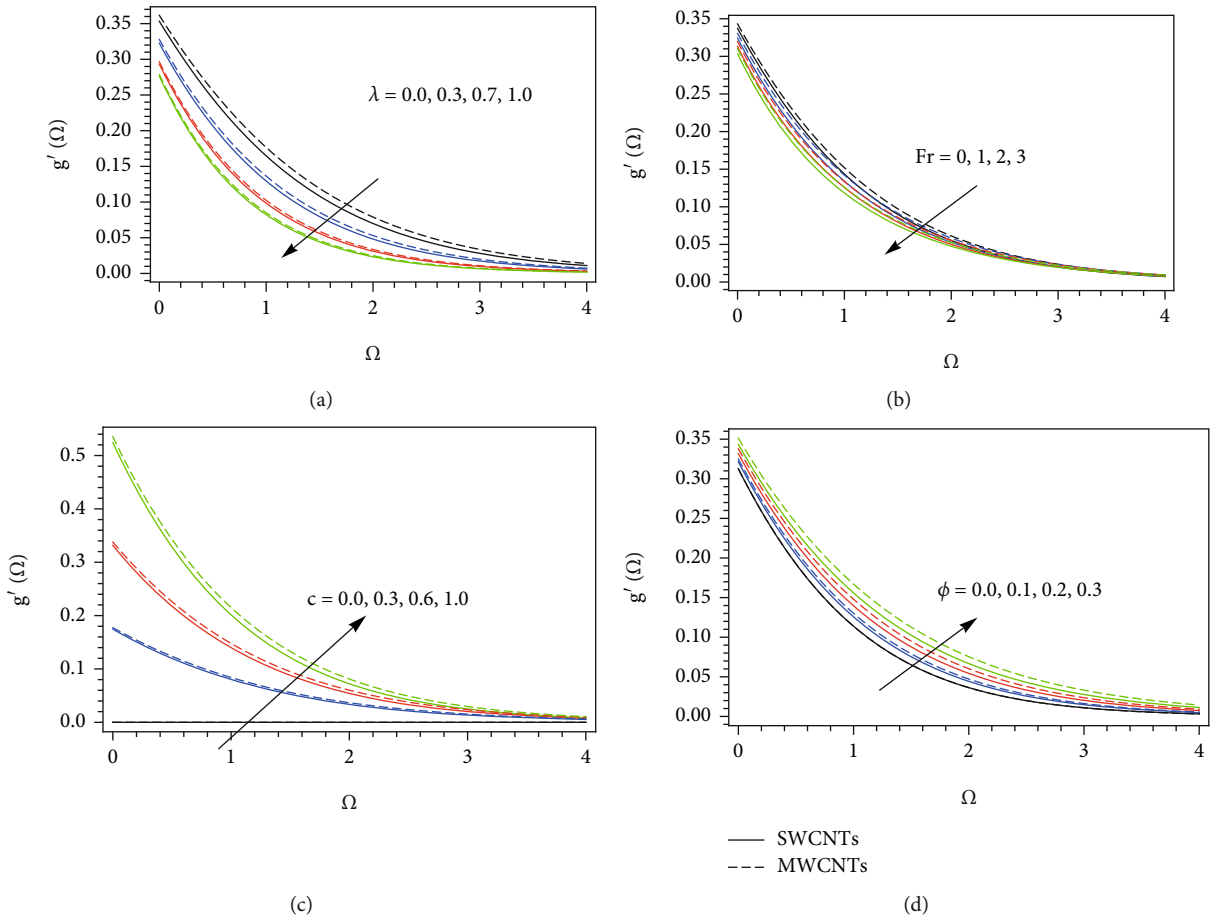

Figure 4: The y-direction velocity for distinct quantity of λ (a), Fr (b), c (c), and ϕ (d).

and Subbarayudu et al. [47]):

$$u = U_w = ax + \frac{2-\sigma_v}{\sigma_v}\lambda_0\frac{\partial u}{\partial z}; v = V_w = by + \frac{2-\sigma_v}{\sigma_v}\lambda_0\frac{\partial v}{\partial z};$$
$$w = 0; -k_{nf}\frac{\partial T}{\partial z} = h_c\left[T_f - T\right] \text{ at } z = 0,$$
$$u \longrightarrow 0; v \longrightarrow 0; T \longrightarrow T_\infty \text{ as } z \longrightarrow \infty. \tag{5}$$

All notations are given in the nomenclature part.

The thermophysical properties of dynamic viscosity, density, heat capacitance of the nanofluid, thermal diffusivity, and thermal conductivity are mathematically expressed as

$$\frac{\mu_{nf}}{\mu_f} = \frac{1}{(1-\phi)^{2.5}}; \frac{\rho_{nf}}{\rho_f} = 1-\phi+\phi\frac{\rho_{CNT}}{\rho_f}; \frac{(\rho c_p)_{nf}}{(\rho c_p)_f} = 1-\phi+\phi\frac{(\rho c_p)_{\text{CNT}}}{(\rho c_p)_f},$$
$$\alpha_{nf} = \frac{k_{nf}}{(\rho c_p)_{nf}}; \frac{k_{nf}}{k_f} = \frac{1-\phi+2\phi\left(k_{\text{CNT}}/\left(k_{\text{CNT}}-k_f\right)\right)\ln\left(\left(k_{\text{CNT}}+k_f\right)/2k_f\right)}{1-\phi+2\phi\left(k_f/\left(k_{\text{CNT}}-k_f\right)\right)\ln\left(\left(k_{\text{CNT}}+k_f\right)/2k_f\right)}. \tag{6}$$

Define

$$u = axf', v = ayg', w = -\sqrt{av_f}[f+g], \Omega = \sqrt{\frac{a}{v_f}}z, \theta = \frac{T-T_\infty}{T_f-T_\infty}. \tag{7}$$

Applying equation (7) in equations (2)–(4), we get

$$A_1A_2f''' - f'^2 + [f+g]f'' - A_1A_2\lambda f' - \text{Fr}f'^2 + \text{Ha}A_2\text{Exp}[-\beta\Omega] = 0, \tag{8}$$

$$A_1A_2g''' - g'^2 + [f+g]g'' - A_1A_2\lambda g' - \text{Fr}g'^2 = 0, \tag{9}$$

$$\frac{A_3}{\text{Pr}A_4}\theta'' + [f+g]\theta' - \Gamma\left([f+g]^2\theta'' + [f+g]\left[f'+g'\right]\theta'\right)$$
$$+ \frac{\text{Hg}}{A_4}\theta + \frac{4}{3}R\frac{1}{A_4\text{Pr}}\left[(\Lambda-1)^3\theta^3\theta'' + 3(\Lambda-1)^3\theta^2\theta'^2\right.$$
$$+ 3(\Lambda-1)^2\theta^2\theta'' + 6(\Lambda-1)^2\theta\theta'^2 + 3(\Lambda-1)\theta\theta''$$
$$\left.+ 3(\Lambda-1)\theta'^2 + \theta''\right] = 0. \tag{10}$$

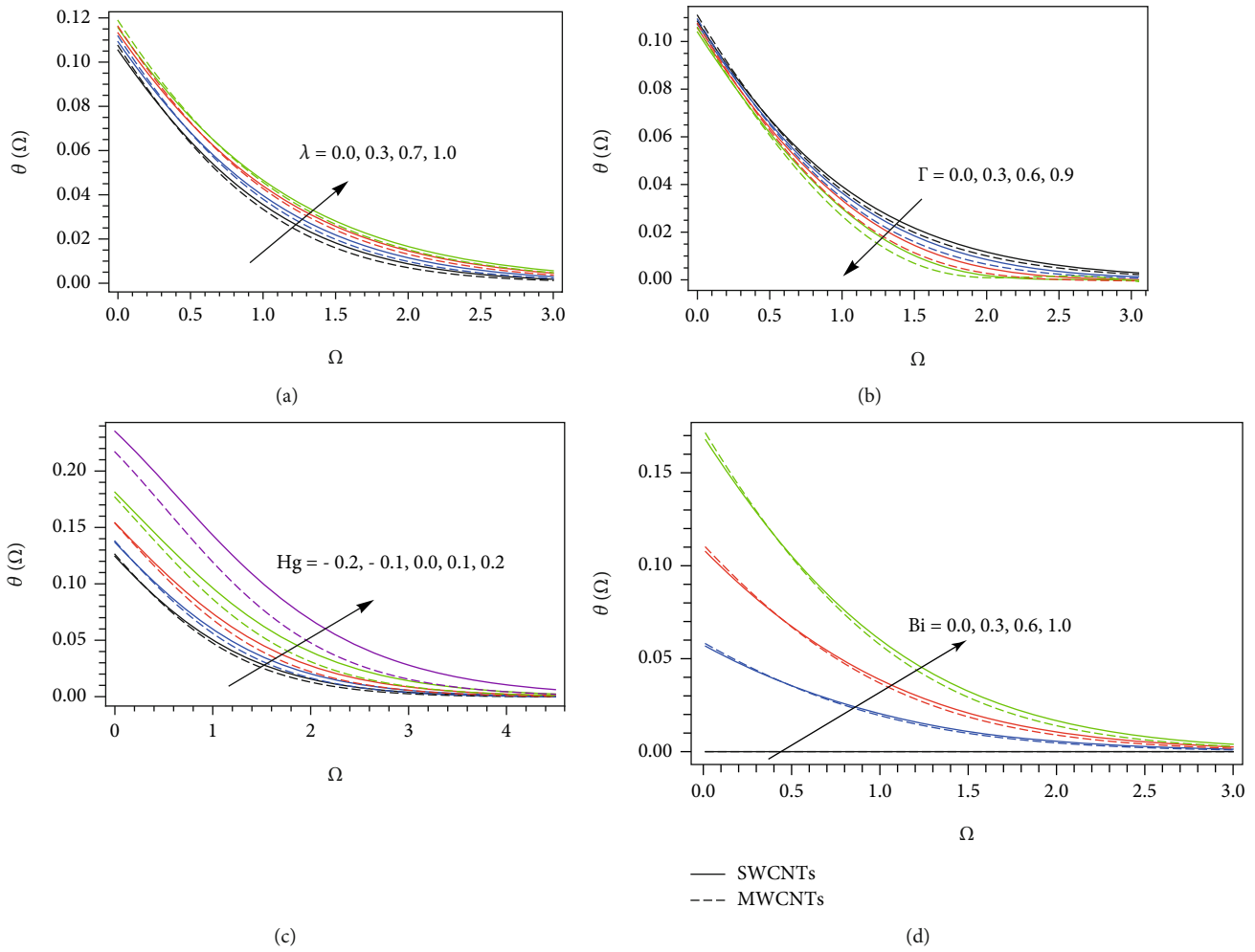

Figure 5: The temperature profile for distinct quantity of λ (a), Γ (b), Hg (c), and Bi (d).

The transferred boundary conditions are

$$f(0)=0\,;f'(0)=1+Kf''(0)\,;f'(\infty)=0\,;g(0)=0, \quad (11)$$

$$g'(0)=c+\mathrm{Kg}''(0)\,;g'(\infty)=0\,;\theta'(0)=-\frac{B_i}{A_3}[1-\theta(0)]\,;\theta(\infty)=0. \quad (12)$$

All parameters are explained in Nomenclature. Here,

$$A_1=\frac{1}{(1-\phi)^{2.5}}\,;A_2=\frac{1}{(1-\phi)+\phi\left(\rho_{\mathrm{CNT}}/\rho_f\right)},$$

$$A_3=\frac{(1-\phi)+2\phi\left(k_{\mathrm{CNT}}/\left(k_{\mathrm{CNT}}-k_f\right)\right)\ln\left(\left(k_{\mathrm{CNT}}+k_f\right)/2k_f\right)}{(1-\phi)+2\phi\left(k_f/\left(k_{\mathrm{CNT}}-k_f\right)\right)\ln\left(\left(k_{\mathrm{CNT}}+k_f\right)/2k_f\right)}\,;$$

$$A_4=(1-\phi)+\phi\frac{\left(\rho c_p\right)_{\mathrm{CNT}}}{\left(\rho c_p\right)_f}. \quad (13)$$

The skin friction coefficients and local Nusselt number are defined as follows:

$$Cfx\sqrt{\mathrm{Re}}=A_1f''(0)\,;Cf_y\sqrt{\mathrm{Re}}=\frac{A_1}{c^{3/2}}g''(0)\,;\frac{\mathrm{Nu}}{\sqrt{\mathrm{Re}}}=-\left[A_3+\frac{4}{3}R\{1+(\Lambda-1)\theta(0)\}^3\right]\theta'(0). \quad (14)$$

3. Entropy Analysis

The entropy generation equation is expressed as (see Hayat et al. [44])

$$S_{\mathrm{gen}}=\frac{k_f}{T_\infty^2}\left[\frac{k_{nf}}{k_f}+\frac{16\sigma^*T^3}{3k_fk^*}\right]\left(\frac{\partial T}{\partial z}\right)^2+\frac{\mu_{nf}}{T_\infty}\left(u^2+v^2\right)+\frac{\mu_{nf}}{T_\infty}\left[\left(\frac{\partial u}{\partial z}\right)^2+\left(\frac{\partial v}{\partial z}\right)^2\right]. \quad (15)$$

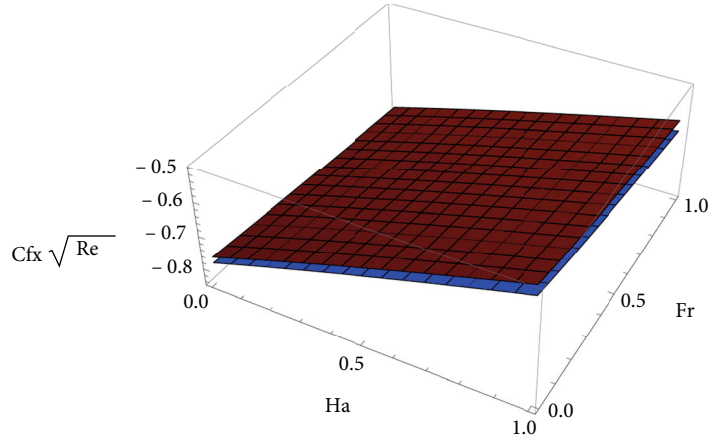

(a)

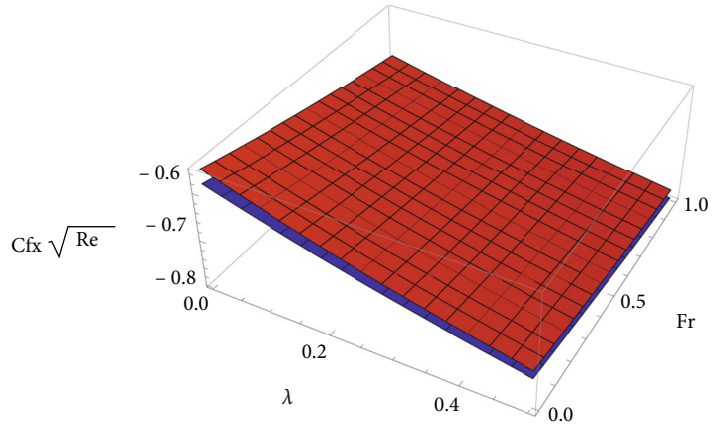

(b)

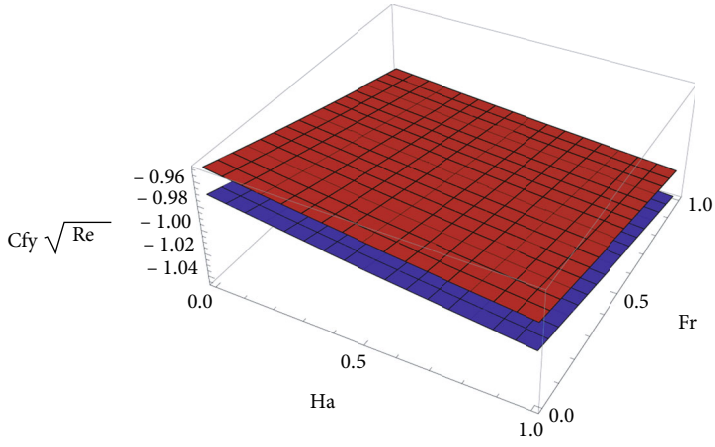

(c)

Figure 6: Continued.

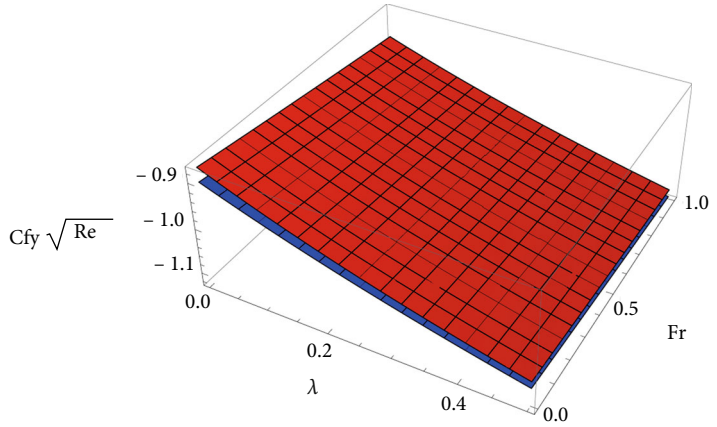

(d)

Figure 6: Skin friction coefficient (lower plate (SWCNTs) and upper plate (MWCNTs)) for different combinations of Ha, Fr, and λ on x -direction (a, b) and y-direction (c, d).

The converted EG equation is

$$\begin{aligned}\text{EG} = A_3\ \text{Re}\,\theta'^2 + \frac{4}{3}R\ \text{Re}\left[(\Lambda-1)^3\theta^3\theta'^2 + 3(\Lambda-1)^2\theta^2\theta'^2\right.\\ \left.+ 3(\Lambda-1)\theta\theta'^2 + \theta'^2\right] + A_1\text{ReBr}\frac{\lambda}{\alpha_1}\left[f'^2 + g'^2\right]\\ + A_1\text{ReBr}\frac{1}{\alpha_1}\left[f''^2 + g''^2\right],\end{aligned} \tag{16}$$

where $\text{Re} = ax^2/\nu_f$ is the local Reynolds number, $\text{Br} = \mu_f a^2 x^2/k_f(T_f - T_\infty)$ is the Brinkman number, and $\alpha_1 = (T_f - T_\infty)/T_\infty$ is the temperature difference parameter.

The Bejan number is expressed as

$$\begin{aligned}\text{BN} &= \frac{\text{Entropy generation due to heat transfer}}{\text{Total entropy generation}},\\ \text{BN} &= \frac{Z_1}{Z_2},\end{aligned} \tag{17}$$

where

$$\begin{aligned}Z_1 = A_3\ \text{Re}\,\theta'^2 + \frac{4}{3}R\ \text{Re}\left[(\Lambda-1)^3\theta^3\theta'^2 + 3(\Lambda-1)^2\theta^2\theta'^2\right.\\ \left.+ 3(\Lambda-1)\theta\theta'^2 + \theta'^2\right],\end{aligned}$$

$$\begin{aligned}Z_2 = A_3\ \text{Re}\,\theta'^2 + \frac{4}{3}R\ \text{Re}\left[(\Lambda-1)^3\theta^3\theta'^2 + 3(\Lambda-1)^2\theta^2\theta'^2\right.\\ \left.+ 3(\Lambda-1)\theta\theta'^2 + \theta'^2\right] + A_1\text{ReBr}\frac{\lambda}{\alpha_1}\left[f'^2 + g'^2\right]\\ + A_1\text{ReBr}\frac{1}{\alpha_1}\left[f''^2 + g''^2\right].\end{aligned} \tag{18}$$

4. Solutions

4.1. Numerical Solutions. The rechanged models ((8)-(10)) with the associated conditions (12) are numerically solved by applying the MATLAB bvp4c algorithm (see Rehman et al. [48] and Eswaramoorthi et al. [49]). To solve these equations, first, we convert higher ODE to first-order ODEs.

$$f = D_1, f' = D_2, f'' = D_3, g = D_4, g' = D_5, g'' = D_6, \theta = D_7, \theta' = D_8. \tag{19}$$

The systems of equations are

$$\begin{aligned}f' &= D_2,\\ f'' &= D_3,\\ f''' &= \frac{D_2^2 - (D_1 + D_4)D_3 - \text{Ha}A_2e^{-\beta\eta} + A_1A_2\lambda D_2 + \text{Fr}D_2^2}{A_1A_2},\\ g' &= D_5,\\ g'' &= D_6,\\ g''' &= \frac{D_5^2 - (D_1 + D_4)D_6 + A_1A_2\lambda D_5 + \text{Fr}D_5^2}{A_1A_2},\\ \theta' &= D_8,\\ \theta'' &= \frac{P_1}{P_2},\end{aligned} \tag{20}$$

where

$$\begin{aligned}P_1 = -\frac{1}{\text{Pr}A_4}\frac{4}{3}R\left[3(\Lambda-1)^3D_7^3D_8^2 + 6(\Lambda-1)^2D_7D_8^2 + 3(\Lambda-1)D_8^2\right]\\ - (D_1 + D_4)D_8 + \Gamma(D_1 + D_4)(D_2 + D_5)D_8 - \frac{\text{Hg}}{A_4}D_7,\\ P_2 = \frac{A_3}{\text{Pr}A_4} - \Gamma(D_1 + D_4)^2\\ + \frac{1}{\text{Pr}A_4}\frac{4}{3}R\left[(\Lambda-1)^3D_7^3 + 3(\Lambda-1)^2D_7^2 + 3(\Lambda-1)D_7 + 1\right].\end{aligned} \tag{21}$$

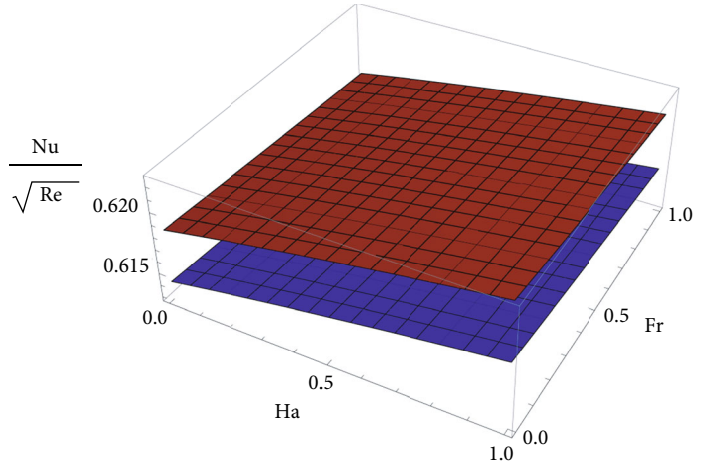

(a)

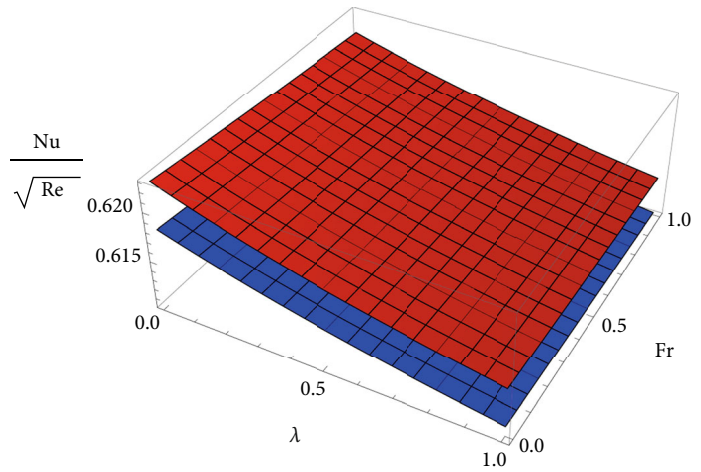

(b)

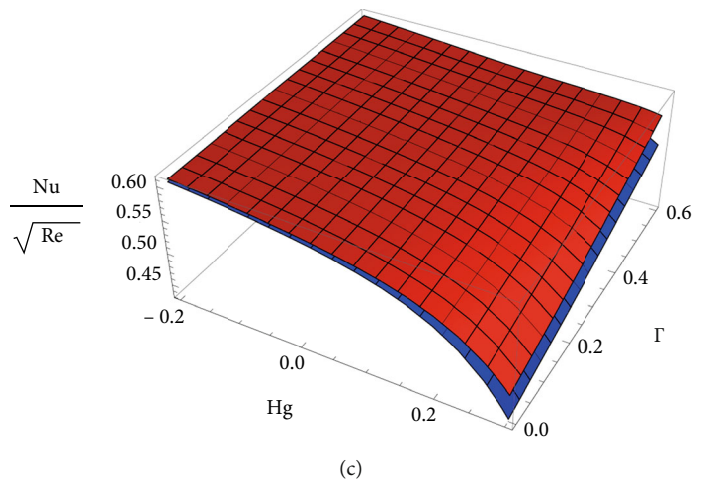

(c)

Figure 7: Continued.

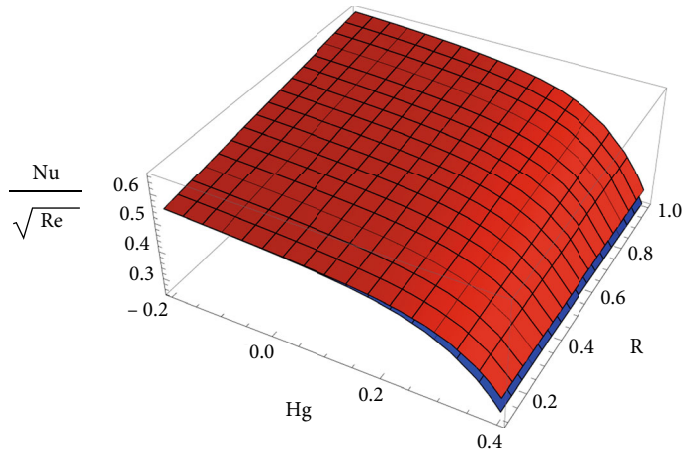

(d)

Figure 7: Local Nusselt number (lower plate (SWCNTs) and upper plate (MWCNTs)) for different combinations of Ha, Fr, λ, Hg, Γ, and R.

With the corresponding conditions,

$$\begin{aligned} &D_1(0) = 0, D_2(0) = 1 + KD_3(0), D_2(\infty) = 0, \\ &D_4(0) = 0, D_5(0) = c + KD_6(0), D_5(\infty) = 0, \\ &D_8(0) = -\frac{Bi}{A_3}[1 - D_7(0)], D_7(\infty) = 0, \end{aligned} \tag{22}$$

4.2. Analytical Solutions. The nonlinear ODE models ((8)-(10)) with conditions (12) are analytically solved by implementing the HAM logic, because this method is a powerful tool for solving highly nonlinear problems (see Gul et al. [50], Islam et al. [51], Saeed et al. [52], and Khan et al. [53]. All computations are made by MATHEMATICA. Initially, we fix the initial approximation as $f_0(\Omega) = (1/(1+K))(1-(1/e^{\Omega}))$, $g_0(\Omega) = (c/(1+K))(1-(1/e^{\Omega}))$, and $\theta_0(\Omega) = \mathrm{Bi}/(\mathrm{Bi}+A_3)e^{\Omega}$, and linear operators are $L_f = D^3 f - Df$, $L_g = D^3 g - Dg$, and $L_\theta = D^2\theta - \theta$, where D is the differential operator, and the property $L_f[X_1 + X_2 e^{\Omega} + X_3(1/e^{\Omega})] = 0 = L_g[X_4 + X_5 e^{\Omega} + X_6(1/e^{\Omega})] = L_\theta[X_7 e^{\Omega} + X_8(1/e^{\Omega})]$, where $X_k(k = 1-8)$ are constants.

After substituting the M^{th}-order HAM, we have

$$\begin{aligned} f_M(\Omega) &= f_M^+(\Omega) + X_1 + X_2 e^{\Omega} + X_3 \frac{1}{e^{\Omega}}, \\ g_M(\Omega) &= g_M^+(\Omega) + X_4 + X_5 e^{\Omega} + X_6 \frac{1}{e^{\Omega}} \\ \theta_M(\Omega) &= \theta_M^+(\Omega) + X_7 e^{\Omega} + X_8 \frac{1}{e^{\Omega}}, \end{aligned} \tag{23}$$

where $f_M^+(\Omega)$, $\theta_M^+(\Omega)$, and $\phi_M^+(\Omega)$ are the particular solutions.

The HAM solutions contain the auxiliary parameters (h_f, h_g, and h_θ), and these act as a key role for solution convergence (see Eswaramoorthi et al. [54] and Loganathan et al. [55]). In SWCNTs, the range values are $-1.4 \le h_f \le -0.1$, $-1.4 \le h_g \le -0.35$, and $-1.5 \le h_\theta \le -0.15$, and MWCNTs are $-1.3 \le h_f \le -0.1$, $-1.15 \le h_g \le -0.1$, and $-1.35 \le h_\theta \le -0.25$ (see Figures 2(a)–2(c). We fix $h_f = h_g = h_\theta = -0.7$ for getting more accuracy in both CNTs.

5. Correlation Equations

The correlation equations are expressed using a recursion formula.

For SWCNTs,

$$\begin{aligned} Cfx\sqrt{\mathrm{Re}} &= -0.5751 - 1.7388\phi - 0.2239\lambda - 0.0653\mathrm{Fr} \\ &\quad + 0.2325\mathrm{Ha} - 0.0307c + 0.2032K, \\ Cfy\sqrt{\mathrm{Re}} &= -1.289 - 2.3097\phi - 0.2520\lambda - 0.0305\mathrm{Fr} \\ &\quad - 0.0249\mathrm{Ha} + 0.8516c + 0.2889K, \\ \frac{\mathrm{Nu}}{\sqrt{\mathrm{Re}}} &= -0.0276 - 0.7926\phi - 0.0124\lambda - 0.0045\mathrm{Fr} + 0.0036\mathrm{Ha} \\ &\quad + 0.0075c - 0.0052 - 0.1630\mathrm{Hg} + 0.1238R + 1.1152\mathrm{Bi}. \end{aligned} \tag{24}$$

For MWCNTs,

$$\begin{aligned} Cfx\sqrt{\mathrm{Re}} &= -0.5704 - 1.6028\phi - 0.243\lambda - 0.0646\mathrm{Fr} \\ &\quad + 0.2433\mathrm{Ha} - 0.03c + 0.1936K, \\ Cfy\sqrt{\mathrm{Re}} &= -1.2696 - 2.1782\phi - 0.2722\lambda - 0.0296\mathrm{Fr} \\ &\quad - 0.0244\mathrm{Ha} + 0.8372c + 0.2786K, \\ \frac{\mathrm{Nu}}{\sqrt{\mathrm{Re}}} &= 0.0299 - 0.8036\phi - 0.0084\lambda - 0.0020\mathrm{Fr} + 0.0039\mathrm{Ha} \\ &\quad + 0.0081c - 0.0034K - 0.1277\mathrm{Hg} + 0.0443R + 1.1217\mathrm{Bi}, \end{aligned} \tag{25}$$

where $\phi \in [0,0.3]$, $\lambda, \mathrm{Fr}, \mathrm{Ha}, c \in [0,1]$, $K \in [0.5,3]$, $\mathrm{Hg} \in [-0.6,0.3]$, $R \in [0,2]$, and $\mathrm{Bi} \in [-0.6,0.6]$ with maximum error difference of 0.099.

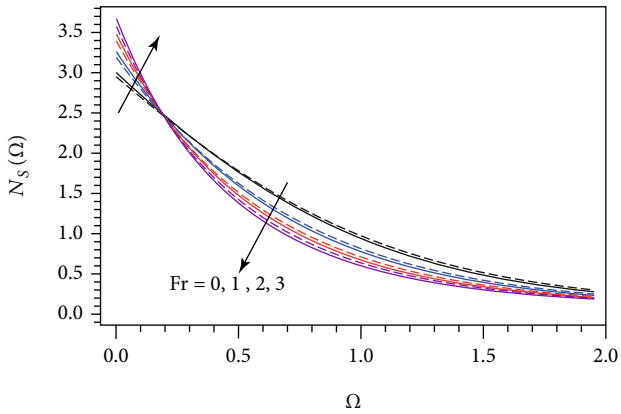

(a)

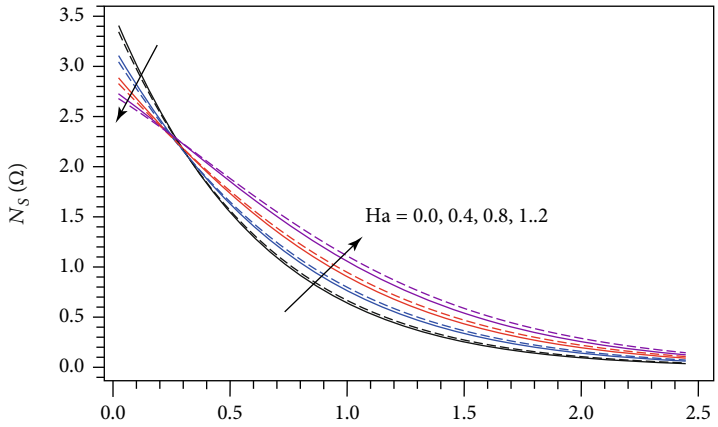

(b)

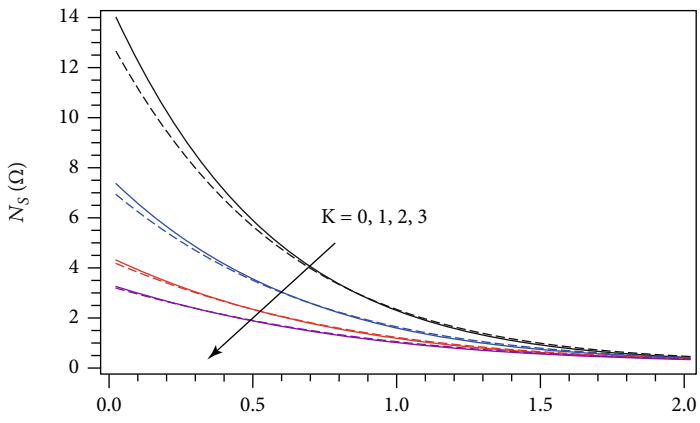

(c)

Figure 8: Continued.

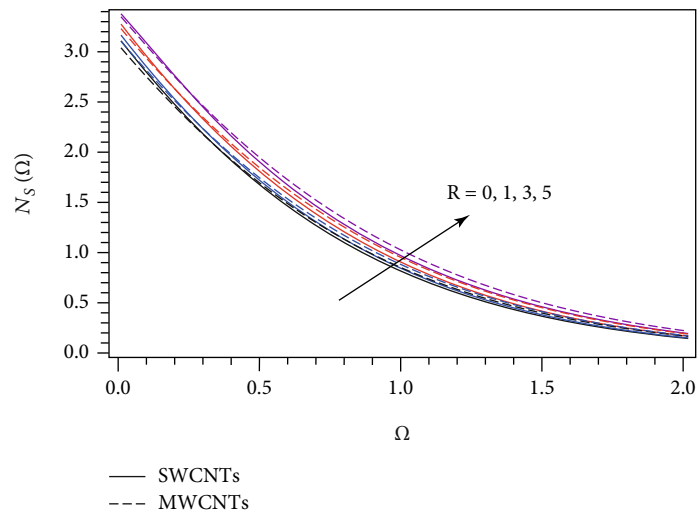

(d)

Figure 8: The entropy generation profile for distinct quantity of Fr (a), Ha (b), K (c), and R (d).

6. Results and Discussion

In this section, we explain the characteristics of flow parameters on velocity ($f'(\Omega)$ and $g'(\Omega)$), temperature ($\theta(\Omega)$), skin friction coefficients ($Cfx\sqrt{\mathrm{Re}}$ and $Cfy\sqrt{\mathrm{Re}}$), local Nusselt number ($\mathrm{Nu}/\sqrt{\mathrm{Re}}$), entropy generation ($N_s(\Omega)$), and Bejan number (BN) through diagrams and tables. Table 1 provides the thermophysical properties of single-wall carbon nanotubes (SWCNTs), multiwall carbon nanotube (MWCNTs), and glycerin. The disparate order of HAM is presented in Table 2. From this table, we acknowledged that the 14^{th} order is enough for all computations. The comparison of Cfx and Cfy with Hayat et al. [56] for different c values is illustrated in Table 3. It is seen that our numerical and HAM results are exactly matched with Hayat et al. [56] results. Tables 4 and 5 portrays the impact of λ, Fr, Ha, c, K, and ϕ on skin friction coefficients ($Cfx\sqrt{\mathrm{Re}}$ and $Cfy\sqrt{\mathrm{Re}}$) for both CNTs. It is detected that the surface drag force $Cfx\sqrt{\mathrm{Re}}$ decays when improving the quantity of λ, Fr, c, and ϕ, and it enhances when raising the values of Ha and K. Also, $Cfy\sqrt{\mathrm{Re}}$ downfalls when strengthening the presence of λ, Fr, Ha, and ϕ, and it improves when enriching the magnitude of c and K for both CNTs. The local Nusselt number for disparate values of Ha, c, K, ϕ, Hg, R, Bi, Γ, and Λ for both CNTs is illustrated in Table 6. It proved that the heat transfer gradient upsurges for enlarging the Ha, c, R, Γ, Λ, and Bi values, and it slumps when raising the values of K, ϕ, and Hg for both CNTs.

Figures 3(a)–3(d) display the consequences of λ, Fr, Ha, and ϕ on the x-direction velocity profile. It is noticed that the x-direction velocity exalts when escalating the quantity of Ha and ϕ, and its downfalls when raising the values of λ and Fr. The effectuates of λ, Fr, c, and ϕ on the y-direction velocity profile are shown in Figures 4(a)–4(d). It is noted that the y-direction velocity surges when enhancing the amount of c and ϕ, and it decays when raising the values of λ and Fr. Physically, the higher amount of porosity leads to enriching the fluid resistance, which suppresses the fluid motion and reduces the corresponding boundary layer thickness. From Figures 5(a)–5(d), it is concluded that the fluid temperature booms up when adding more quantities of λ, Hg, and Bi, and it weakens when strengthening the Γ values. The larger magnitude of the Biot number leads to enhancing the heat transfer coefficient, and this causes to reinforce the fluid warmness, which leads to the thickening of the thermal boundary layer. Figures 6(a)–6(d) illustrate the outcomes of Ha, Fr, and λ on skin friction coefficients ($Cfx\sqrt{\mathrm{Re}}$ and $Cfy\sqrt{\mathrm{Re}}$). It is seen that the $Cfx\sqrt{\mathrm{Re}}$ rises when raising the Ha values, and the opposite behavior was attained for more presence of Fr and λ. Also, Ha, Fr, and λ leads to suppressing the $Cfy\sqrt{\mathrm{Re}}$. In addition, the surface shear stress is lower in SWCNTs than in MWCNTs. The local Nusselt number for different combinations of Ha, Fr, λ, Hg, Γ, and R is plotted in Figures 7(a)–7(d). It is proven that the heat transfer gradient ascents when enriching the Ha, Γ, and R, and it declines when increasing the λ, Fr, and Hg values. The larger values of the radiation parameter enhance the heat transfer rate from high-temperature places to low-temperature places, and this causes to rise in the heat transfer gradient. In addition, a higher heat transfer gradient occurs in MWCNTs compared to SWCNTs. Figures 8(a)–8(d) delineate the effects of Fr, Ha, K, and R on the entropy generation profile. It is noticed that the entropy generation profile increases (decreases) near the plate, and it diminishes (grows) away from the plate for changing the Fr (Ha) values. The entropy generation profile enhances when enriching the radiation parameter, and it weakens when raising the slip parameter. The variations of the Bejan number for disparate values of Bi, Hg, K, and R are presented in Figures 9(a)–9(d). It is exposed that the Bejan number progresses when upgrading the magnitude of Bi, Hg, K, and R.

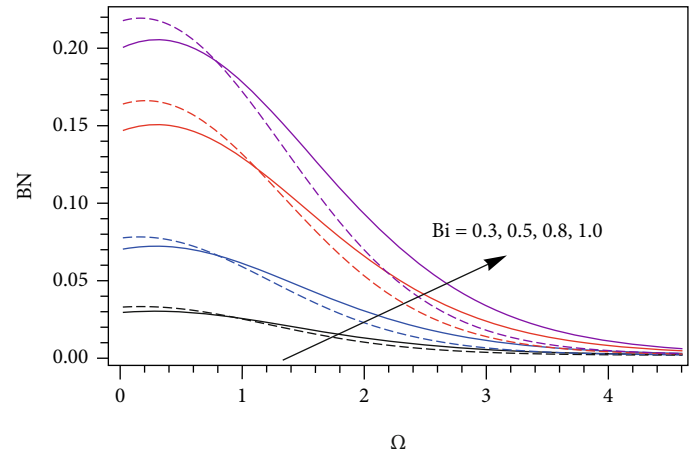

(a)

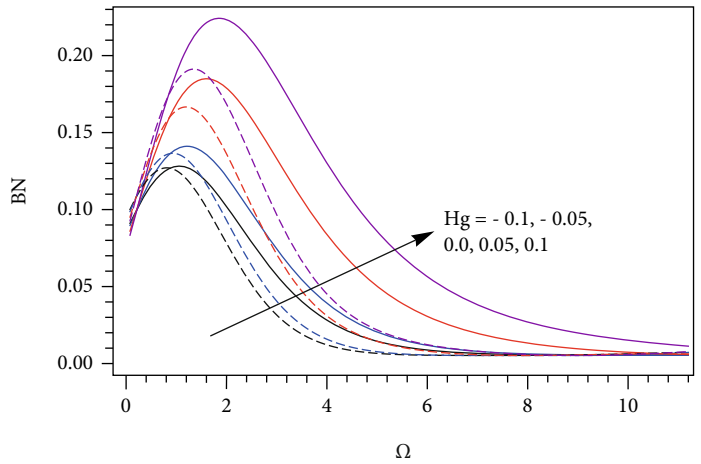

(b)

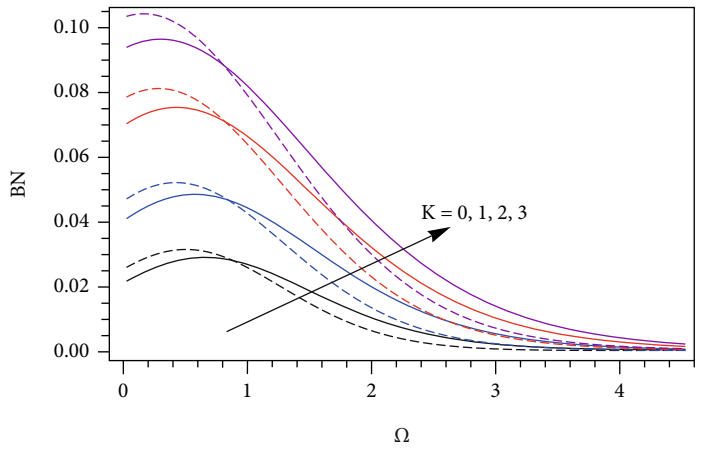

(c)

Figure 9: Continued.

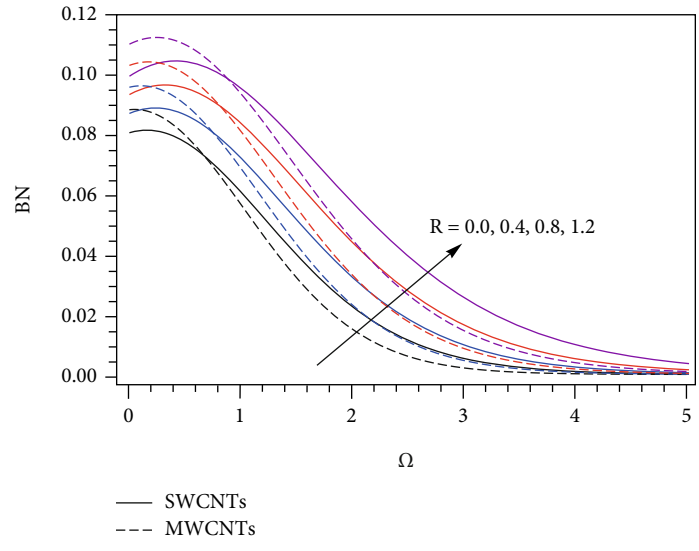

(d)

Figure 9: The Bejan number profile for distinct quantity of Bi (a), Hg (b), K (c), and R (d).

7. Conclusions

Here, we provide the impact of the Darcy-Forchheimer flow of glycerin-based carbon nanotubes with velocity slip over a heated Riga plate with heat absorption/generation. The Cattaneo-Christov heat flux theory is used to formulate the energy equation. In addition, nonlinear facets of radiation are also included in the energy expression. The obtained flow models are converted into an ODE model with the help of suitable variables. The ODE models are solved numerically and analytically by applying MATLAB bvp4c and HAM ideas, respectively. The main outputs of our investigation are summarized below:

(i) The fluid motion in both directions is suppressed when adding more quantity of porosity parameter and Forchheimer number

(ii) The fluid temperature aggravates when enriching the heat absorption/generation and convective heating parameters

(iii) Both porosity parameter and Forchheimer number lead to curtailing the surface shear stress in both directions

(iv) The thermal relaxation time parameter leads to exaggerating the heat transfer gradient, and heat absorption/generation parameters act opposite to the local Nusselt number

(v) The thermal radiation parameter boosts up the entropy generation, and the slip parameter helps to cut down the entropy generation

(vi) The Bejan number upgrades when there is more quantity of the Biot number and radiation parameter

Nomenclature

a, b:	Positive constants (s^{-1})
α:	Thermal diffusivity ($m^2\ s^{-1}$)
a_1:	Magnets positioned in the interval separating the electrodes (-)
$Cfx\sqrt{\mathrm{Re}}$&$Cfy\sqrt{\mathrm{Re}}$:	Skin friction coefficients (-)
c_p:	Capacity of specific heat ($m^2\ s^{-2}$) K^{-1}
F:	Inertia coefficient of porous medium (-)
h_c:	Heat transfer coefficient (-)
J_0:	Current density applied to the electrodes (Am^{-2})
$k*$:	Thermal conductivity (-)
M:	Magnetic property of the permanent magnets that are organized on top of the plate surface ($kg\,s^{-2}\,A^{-1}$)
nf, f:	Subscript represents nanofluid and base fluid
ν:	Kinematic viscosity ($m^2\,s^{-1}$)
Ω:	Dimensionless variable
Q:	Heat consumption/generation coefficient ($Wm^{-3}\,K^{-1}$)
ρ:	Fluid density ($kg\,m^{-3}$)
T:	Nondimensional temperature (K)
T_f:	Temperature of the hot fluid (K)
T_w:	Surface temperature (K)
T_∞:	Ambient temperature (K)
τ_w:	Surface shear stress
θ:	Dimensionless temperature
u, v, w:	Velocity components
U_w, V_w:	Surface stretching velocities ($m^2\,s^{-1}$)
x, y, z:	Cartesian coordinates (m)
$\alpha_1 (= T_f - T_\infty / T_\infty)$:	Temperature difference parameter
$\mathrm{Bi} (= (h_c/k_f)\sqrt{v_f/a})$:	Biot number

$\beta(=(\pi/a_1)\sqrt{\nu_f/a})$: Dimensionless parameter
$\mathrm{Br}(=\mu_f a^2x^2/k_f(T_f - T_\infty))$: Brinkman number
$\mathrm{Fr}(=c_b/\sqrt{k_1^*})$: Forchheimer number
$\Gamma(=\lambda a)$: Thermal relaxation time parameter
$\mathrm{Ha}(=\pi J_0 M/8\rho_f a^2 x)$: Modified Hartmann number
$\mathrm{Hg}(=Q/(\rho c_p)_f a)$: Heat consumption/generation parameter
$\Lambda(=\nu_f/k_1^* a)$: Porosity parameter
$\mathrm{Pr}(=(\mu c_p)_f/k_f)$: Prandtl number
$\mathrm{Re}\ (=ax^2/\nu_f)$: Local Reynolds number.

Abbreviations

HAM: Homotopy analysis method
CNTs: Carbon nanotubes
ODE: Ordinary differential equations
MHD: Magnetohydrodynamics
MWCNTs: Multiwall carbon nanotubes
SWCNTs: Single-wall carbon nanotubes.

Data Availability

The raw data supporting the conclusions of this article will be made available by the corresponding author without undue reservation.

Conflicts of Interest

The authors declare that they have no competing interests.

Authors' Contributions

All authors contributed equally to this work. And all the authors have read and approved the final version manuscript.

References

[1] R. Kamali and A. R. Binesh, "Numerical investigation of heat transfer enhancement using carbon nanotube- based non-Newtonian nanofluids," *International Communications in Heat and Mass Transfer*, vol. 37, no. 8, pp. 1153–1157, 2010.

[2] S. Harish, K. Ishikawa, E. Einarsson et al., "Enhanced thermal conductivity of ethylene glycol with single-walled carbon nanotube inclusions," *International Journal of Heat and Mass Transfer*, vol. 55, pp. 3885–3890, 2012.

[3] R. U. Haq, S. Nadeem, Z. H. Khan, and N. F. M. Noor, "Convective heat transfer in MHD slip flow over a stretching surface in the presence of carbon nanotubes," *Physica B: Condensed Matter*, vol. 457, pp. 40–47, 2015.

[4] D. Lu, M. Ramzan, S. Ahmad, J. D. Chung, and U. Farooq, "Upshot of binary chemical reaction and activation energy on carbon nanotubes with Cattaneo-Christov heat flux and buoyancy effects," *Physics of Fluids*, vol. 29, 2017.

[5] A. U. Rehman, R. Mehmood, S. Nadeem, N. S. Akbar, and S. S. Motsa, "Effects of single and multi-walled carbon nanotubes on water and engine oil based rotating fluids with internal heating," *Advanced Powder Technology*, vol. 28, no. 9, pp. 1991–2002, 2017.

[6] P. Sreedevi, P. S. Reddy, and A. J. Chamkha, "Magneto-hydrodynamics heat and mass transfer analysis of single and multi-wall carbon nanotubes over vertical cone with convective boundary condition," *International Journal of Mechanical Sciences*, vol. 135, pp. 646–655, 2018.

[7] D. Lu, Z. Li, M. Ramzan, A. Shafee, and J. D. Chung, "Unsteady squeezing carbon nanotubes based nano-liquid flow with Cattane-Christov heat flux and homogeneous-heterogeneous reactions," *Applied Nanoscience*, vol. 9, no. 2, pp. 169–178, 2019.

[8] M. Bilal, A. Saeed, T. Gul, I. Ali, W. Kumam, and P. Kumam, "Numerical approximation of microorganisms hybrid nano-fluid flow induced by a wavy fluctuating spinning disc," *Coatings*, vol. 11, no. 9, 2021.

[9] T. Gul, M. Usman, I. Khan et al., "Magneto hydrodynamic and dissipated nanofluid flow over an unsteady turning disk," *Advances in Mechanical Engineering*, vol. 13, no. 7, 2021.

[10] P. Forchheimer, "Wasserbewegung durch boden," *Zeitschrift fur Acker und Pflanzenbau*, vol. 45, pp. 1782–1788, 1901.

[11] S. A. Bakar, N. M. Arifin, R. Nazar, F. M. Ali, and I. Pop, "Forced convection boundary layer stagnation-point flow in Darcy-Forchheimer porous medium past a shrinking sheet," *Frontiers Heat and Mass Transfer*, vol. 7, no. 1, pp. 1–7, 2016.

[12] J. C. Umavathi, O. Ojjela, and K. Vajravelu, "Numerical analysis of natural convective flow and heat transfer of nanofluids in a vertical rectangular duct using Darcy-Forchheimer-Brinkman model," *International Journal of Thermal Sciences*, vol. 111, pp. 511–524, 2017.

[13] T. Hayat, F. Haider, T. Muhammad, and B. Ahmad, "Darcy-Forchheimer flow of carbon nanotubes due to a convectively heated rotating disk with homogeneous-heterogeneous reactions," *Journal of Thermal Analysis and Calorimetry*, vol. 137, no. 6, pp. 1939–1949, 2019.

[14] M. Ramzan and N. Shaheen, "Thermally stratified Darcy Forchheimer nanofluid flow comprising carbon nanotubes with effects of Cattaneo-Christov heat flux and homogeneous-heterogeneous reactions," *Physica Scripta*, vol. 95, no. 1, 2020.

[15] G. Rasool, A. Shafiq, M. S. Alqarni, A. Wakif, I. Khan, and M. S. Bhutta, "Numerical scrutinization of Darcy-Forchheimer relation in convective magnetohydrodynamic nanofluid flow bounded by nonlinear stretching surface in the perspective of heat and mass transfer," *Micromachines*, vol. 12, no. 4, p. 374, 2021.

[16] M. K. Nayak, S. Shaw, M. I. Khan, V. S. Pandey, and M. Nazeer, "Flow and thermal analysis on Darcy-Forchheimer flow of copper-water nanofluid due to a rotating disk: a static and dynamic approach," *Journal of Materials Research and Technology*, vol. 9, no. 4, pp. 7387–7408, 2020.

[17] A. Saeed, P. Kumam, T. Gul, W. Alghamdi, W. Kumam, and A. Khan, "Darcy-Forchheimer couple stress hybrid nanofluids flow with variable fluid properties," *Scientific Reports*, vol. 11, no. 1, pp. 1–13, 2021.

[18] E. N. Maraj, Z. Khatoon, S. Ijaz, and R. Mehmood, "Effect of Arrhenius activation energy and medium porosity on mixed convective diluted ethylene glycol nanofluid flow towards a curved stretching surface," *International Communications in Heat and Mass Transfer*, vol. 129, pp. 1–9, 2021.

[19] R. Mehmood, S. Khan, E. N. Maraj, S. Ijaz, and S. Rana, "Heat transport mechanism via ion-slip and hall current in

viscoplastic flow along a porous elastic sheet," *Proceedings of the Institution of Mechanical Engineers Part E: Journal of Process Mechanical Engineering*, 2021.

[20] F. Mabood and K. Das, "Melting heat transfer on hydromagnetic flow of a nanofluid over a stretching sheet with radiation and second-order slip," *The European Physical Journal Plus*, vol. 131, pp. 1–12, 2016.

[21] M. Ramzan, J. Chung, and N. Ullah, "Radiative magnetohydrodynamic nanofluid flow due to gyrotactic microorganisms with chemical reaction and nonlinear thermal radiation," *International Journal of Mechanical Sciences*, vol. 130, pp. 31–40, 2017.

[22] M. Usman, M. Hamid, T. Zubair, R. U. Haq, and W. Wang, "Cu-Al_2O_3/Water hybrid nanofluid through a permeable surface in the presence of nonlinear radiation and variable thermal conductivity via LSM," *International Journal of Heat and Mass Transfer*, vol. 126, pp. 1347–1356, 2018.

[23] H. Waqas, S. U. Khan, S. A. Shehzad, and M. Imran, "Significance of the nonlinear radiative flow of micropolar nanoparticles over porous surface with a gyrotactic microorganism, activation energy, and Nield's condition," *Heat Transfer-Asian Research*, vol. 48, no. 7, pp. 3230–3256, 2019.

[24] S. U. Khan, S. A. Shehzad, A. Rauf, and Z. Abbas, "Thermally developed unsteady viscoelastic micropolar nanofluid with modified heat/mass fluxes: a generalized model," *Physica A: Statistical Mechanics and its Applications*, vol. 550, article 123986, 2020.

[25] Y. Li, H. Waqas, M. Imran, U. Farooq, F. Mallawi, and I. Tlili, "A numerical exploration of modified second-grade nanofluid with motile microorganisms, thermal radiation, and Wu's slip," *Symmetry*, vol. 12, no. 3, p. 393, 2020.

[26] T. Muhammad, H. Waqas, S. A. Khan, R. Ellahi, and S. M. Sait, "Significance of nonlinear thermal radiation in 3D Eyring-Powell nanofluid flow with Arrhenius activation energy," *Journal of Thermal Analysis and Calorimetry*, vol. 143, pp. 929–944, 2021.

[27] M. I. Khan, H. Waqas, S. U. Khan et al., "Slip flow of micropolar nanofluid over a porous rotating disk with motile microorganisms, nonlinear thermal radiation and activation energy," *International Communications in Heat and Mass Transfer*, vol. 122, article 105161, 2021.

[28] U. Farooq, H. Waqas, M. I. Khan, S. U. Khan, Y. M. Chu, and S. Kadry, "Thermally radioactive bioconvection flow of Carreau nanofluid with modified Cattaneo-Christov expressions and exponential space-based heat source," *Alexandria Engineering Journal*, vol. 60, no. 3, pp. 3073–3086, 2021.

[29] Z. Shah, P. Kumam, and W. Deebani, "Radiative MHD Casson nanofluid flow with activation energy and chemical reaction over past nonlinearly stretching surface through entropy generation," *Scientific Reports*, vol. 10, no. 1, pp. 1–14, 2020.

[30] A. Bejan, "A study of entropy generation in fundamental convective heat transfer," *Journal of Heat Transfer*, vol. 101, no. 4, pp. 718–725, 1979.

[31] O. D. Makinde and A. S. Eegunjobi, "Entropy analysis of thermally radiating magneto-hydrodynamics slip flow of Casson fluid in a microchannel filled with saturated porous media," *Journal of Porous Media*, vol. 19, no. 9, pp. 799–810, 2016.

[32] M. M. Bhatti, T. Abbas, and M. M. Rashidi, "Numerical study of entropy generation with nonlinear thermal radiation on magnetohydrodynamics non-Newtonian nano fluid through a porous shrinking sheet," *Journal of Magnetics*, vol. 21, pp. 468–475, 2016.

[33] M. M. Rashidi, S. Bagheri, E. Momoniat, and N. Freidoonimehr, "Entropy analysis of convective MHD flow of third grade non-Newtonian fluid over a stretching sheet," *Ain Shams Engineering Journal*, vol. 8, no. 1, pp. 77–85, 2017.

[34] Q. Y. Zhu, Y. J. Zhuang, and H. Z. Yu, "Entropy generation due to three-dimensional double-diffusive convection of power-law fluids in heterogeneous porous media," *International Journal of Heat and Mass Transfer*, vol. 106, pp. 61–82, 2017.

[35] S. Jain and P. Gupta, "Entropy generation analysis of carbon nanotubes nanofluid 3D flow along a nonlinear inclined stretching sheet through porous media," *International Journal of Heat and Technology*, vol. 37, no. 1, pp. 131–138, 2019.

[36] M. Ramzan, M. Mohammad, F. Howari, and J. D. Chung, "Entropy analysis of carbon nanotubes based nanofluid flow past a vertical cone with thermal radiation," *Entropy*, vol. 21, no. 7, p. 642, 2019.

[37] M. Ramzan, M. Mohammad, and F. Howari, "Magnetized suspended carbon nanotubes based nanofluid flow with bioconvection and entropy generation past a vertical cone," *Scientific Reports*, vol. 9, no. 1, pp. 1–15, 2019.

[38] A. Khan, Z. Shah, E. Alzahrani, and S. Islam, "Entropy generation and thermal analysis for rotary motion of hydromagnetic Casson nanofluid past a rotating cylinder with Joule heating effect," *International Communications in Heat and Mass Transfer*, vol. 119, article 104979, 2020.

[39] S. Eswaramoorthi, S. Divya, M. Faisal, and N. Namgyel, "Entropy and Heat Transfer Analysis for MHD Flow of -Water-Based Nanofluid on a Heated 3D Plate with Nonlinear Radiation," *Mathematical Problems in Engineering*, vol. 2022, Article ID 7319988, 14 pages, 2022.

[40] K. Loganathan, K. Mohana, M. Mohanraj, P. Sakthivel, and S. Rajan, "Impact of third-grade nanofluid flow across a convective surface in the presence of inclined Lorentz force: an approach to entropy optimization," *Journal of Thermal Analysis and Calorimetry*, vol. 144, no. 5, pp. 1935–1947, 2021.

[41] P. Y. Xiong, Y. M. Chu, M. I. Khan, S. A. Khan, and S. Z. Abbas, "Entropy optimized Darcy-Forchheimer flow of Reiner-Philippoff fluid with chemical reaction," *Computational and Theoretical Chemistry*, vol. 1200, article 113222, 2021.

[42] S. Rana, R. Mehmood, and S. Nadeem, "Bioconvection through interaction of Lorentz force and gyrotactic microorganisms in transverse transportation of rheological fluid," *Journal of Thermal Analysis and Calorimetry*, vol. 145, no. 5, pp. 2675–2689, 2021.

[43] R. J. Punith Gowda, F. S. Al-Mubaddel, R. Naveen Kumar et al., "Computational modelling of nanofluid flow over a curved stretching sheet using Koo-Kleinstreuer and Li (KKL) correlation and modified Fourier heat flux model," *Chaos, Solitons and Fractals*, vol. 145, article 110774, 2021.

[44] T. Hayat, M. I. Khan, T. A. Khan, M. I. Khan, S. Ahmad, and A. Alsaedi, "Entropy generation in Darcy-Forchheimer bidirectional flow of water-based carbon nanotubes with convective boundary condition," *Journal of Molecular Liquids*, vol. 265, pp. 629–638, 2018.

[45] T. Hayat, M. Imtiaz, A. Alsaedi, and M. A. Kutbi, "MHD three-dimensional flow of nanofluid with velocity slip and nonlinear thermal radiation," *Journal of Magnetism and Magnetic Materials*, vol. 396, no. 15, pp. 31–37, 2015.

[46] A. Zeeshan, Z. Ali, M. R. Gorji, F. Hussain, and S. Nadeem, "Flow analysis of biconvective heat and mass transfer of two-dimensional couple stress fluid over a paraboloid of

revolution," *International Journal of Modern Physics B*, vol. 34, no. 11, 2020.

[47] K. Subbarayudu, S. Suneetha, P. Bala Anki Reddy, and A. M. Rashad, "Framing the activation energy and binary chemical reaction on CNT's with Cattaneo-Christov heat diffusion on Maxwell nanofluid in the presence of nonlinear thermal radiation," *Arabian Journal for Science and Engineering*, vol. 44, no. 12, pp. 10313–10325, 2019.

[48] A. Rehman, Z. Salleh, and T. Gul, "Heat transfer of thin film flow over an unsteady stretching sheet with dynamic viscosity," *Journal of Advanced Research in Fluid Mechanics and Thermal Sciences*, vol. 81, no. 2, pp. 67–81, 2021.

[49] S. Eswaramoorthi, N. Alessa, M. Sangeethavaanee, S. Kayikci, and N. Namgyel, "Mixed convection and thermally radiative flow of MHD Williamson nanofluid with Arrhenius activation energy and Cattaneo-Christov heat-mass flux," *Journal of Mathematics*, vol. 2021, Article ID 2490524, 16 pages, 2021.

[50] T. Gul, M. Rehman, A. Saeed et al., "Magnetohydrodynamic impact on Carreau thin film couple stress nanofluid flow over an unsteady stretching sheet," *Mathematical Problems in Engineering*, vol. 2021, Article ID 8003805, 10 pages, 2021.

[51] S. Islam, A. Khan, P. Kumam et al., "Radiative mixed convection flow of Maxwell nanofluid over a stretching cylinder with Joule heating and heat source/sink effects," *Scientific Reports*, vol. 10, pp. 1–18, 2020.

[52] A. Saeed, P. Kumam, S. Nasir, T. Gul, and W. Kumam, "Nonlinear convective flow of the thin film nanofluid over an inclined stretching surface," *Scientific Reports*, vol. 11, no. 1, pp. 1–15, 2021.

[53] A. Khan, A. Saeed, A. Tassaddiq et al., "Bio-convective and chemically reactive hybrid nanofluid flow upon a thin stirring needle with viscous dissipation," *Scientific Reports*, vol. 11, no. 1, 2021.

[54] S. Eswaramoorthi, N. Alessa, M. Sangeethavaanee, and N. Namgyel, "Numerical and Analytical Investigation for Darcy-Forchheimer Flow of a Williamson Fluid over a Riga Plate with Double Stratification and Cattaneo- Christov Dual Flux," *Advances in Mathematical Physics*, vol. 2021, Article ID 1867824, 15 pages, 2021.

[55] K. Loganathan, N. Alessa, K. Tamilvanan, and F. S. Alshammari, "Significances of Darcy-Forchheimer porous medium in third-grade nanofluid flow with entropy features," *The European Physical Journal Special Topics*, vol. 230, no. 5, pp. 1293–1305, 2021.

[56] T. Hayat, F. Haider, T. Muhammad, and A. Alsaedi, "Darcy-Forchheimer three-dimensional flow of carbon nanotubes with nonlinear thermal radiation," *Journal of Thermal Analysis and Calorimetry*, vol. 140, no. 6, pp. 2711–2720, 2020.